

See discussions, stats, and author profiles for this publication at: <https://www.researchgate.net/publication/278020919>

Shen J.-W., Li C., ven der Velt N. F. A. & Peter C. Understanding the control of mineralization by polyelectrolyte additives: simulation of preferential binding to calcite surfaces...

ARTICLE *in* THE JOURNAL OF PHYSICAL CHEMISTRY C · MARCH 2013

Impact Factor: 4.77 · DOI: 10.1021/jp402341w

CITATIONS

10

READS

9

4 AUTHORS, INCLUDING:



Jia-Wei Shen

Hangzhou Normal University

23 PUBLICATIONS 546 CITATIONS

SEE PROFILE

Understanding the Control of Mineralization by Polyelectrolyte Additives: Simulation of Preferential Binding to Calcite Surfaces

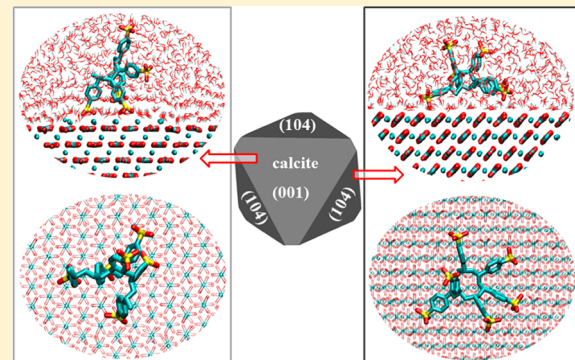
Jia-Wei Shen,[†] Chunli Li,[‡] Nico F. A. van der Vegt,[‡] and Christine Peter^{*,†}

[†]Max Planck Institute for Polymer Research, Ackermannweg 10, D-55128 Mainz, Germany

[‡]Center of Smart Interfaces, Technische Universität Darmstadt, Petersenstrasse 17, D-64287 Darmstadt, Germany

Supporting Information

ABSTRACT: Understanding the mechanisms that govern the crystallization of natural minerals such as calcium carbonate, calcium oxalate, or hydroxyapatite and its control by biological and synthetic polymers can help to guide the design of new biomimetic materials. In this paper, the adsorption behavior of oligomers of polystyrene sulfonate (PSS) on calcite surfaces was investigated by molecular dynamics simulations. The binding strengths of PSS oligomers to different calcite surfaces were computed via potential of mean force calculations, and the binding modes were analyzed in detail. These results could be set in relation to and serve as a molecular-level explanation of the experimentally observed PSS-stabilized exposure of (001) surfaces during calcite mineralization. The simulations show that oligomers of PSS preferentially bind to the polar calcite (001) surface, much stronger than to the nonpolar (104) surface. While sharing in common a dominant role of solvent-induced forces, the mode of binding to the two surfaces is different. The interaction of the sulfonate group with the (001) surface is dominated by both direct and solvent-mediated binding, while the binding of the styrene sulfonate to the (104) surface is mediated by one or two layers of water molecules. Moreover, local solvent density variations at the interface impact the geometry of binding which vastly differs between the two surfaces. In particular, these last effects have important further implications for the preferential binding of PSS polymers (compared to monomers or oligomers) and specific material recognition by synthetic polymers and peptides in general.



1. INTRODUCTION

Many biological materials such as bone, teeth, or nacre exhibit remarkably high strength and toughness in spite of being formed from relatively weak constituents.¹ Multiple studies show that these mechanical properties are mostly due to the hierarchical structuring of the materials at different length scales.^{2–4} In general, these structures are nanoscale composites of stiff inorganic particles which are joined by a soft, elastic organic matrix. For example, nacre has a “brick-and-mortar” structure, in which inorganic calcium carbonate platelets comprise 95 vol. % of the structure, and these ~0.5 μm thick and 5–10 μm wide “bricks” are separated and connected by an organic biopolymer “mortar”.⁵ This soft organic matrix toughens the material, prevents the spread of cracks, and provides elasticity by being reversibly deformable.

Motivated by this excellent mechanical performance of biological materials, plenty of experiments investigated how nanometer-sized mineral particles self-assemble under the mediation of natural biomolecules or synthetic polymers,^{6,7} attempting to mimic the hierarchical organization in naturally occurring materials and to understand in-depth the mechanisms of biomineralization. Calcium carbonate (CaCO_3) is an abundant mineral that provides the basis for skeletal support in marine organisms (such as mollusks and crustaceans) and

also for protection in the shell of avian eggs. In these systems hierarchical structures are formed under precise control of the crystallization and self-organization processes by biopolymers. Therefore, CaCO_3 is an ideal model system to investigate the growth mechanisms of biominerals and bioinspired materials.^{8,9} Experimental strategies to control CaCO_3 crystallization and morphologies involve the use of designed additives to the crystallization process. These additives range from low molecular-weight molecules,^{10,11} to synthetic polymers,^{9,12–14} to biological macromolecules.^{15–17} They can influence different stages of the overall crystallization process, e.g., crystal nucleation or crystal growth. One example for this control of crystal growth is Wang and Cölfen’s work on CaCO_3 crystallization in polystyrene sulfonate (PSS) solution.^{12,13} The presence of PSS during calcite crystallization results in a family of well-defined mesocrystals and a remarkable change from the typical single-crystal calcite rhombohedra with (104) faces to crystals that present the unusual (typically unstable, high-energy) (001) faces. With increasing PSS concentration the (001) face becomes more pronounced. Song and Cölfen also studied CaCO_3 crystallization in the presence of block

Received: March 7, 2013

Published: March 12, 2013



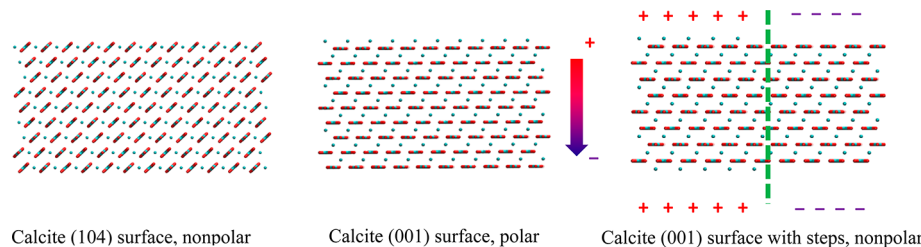


Figure 1. Calcite nonpolar (104) surface, polar (001) surface, and the (001) surface as used in this work: with two steps so that the mineral block is overall nonpolar in the direction normal to the surface (Ca^{2+} ions, cyan dots; CO_3^{2-} ions, cyan and red lines).

poly(4-styrenesulfonate-co-maleic acid) random copolymer, and they found that simple variation of calcium and polyelectrolyte concentrations allows the systematic control of the size and morphology of the formed particles.¹⁴

Despite great progress in understanding the mechanisms of crystal nucleation and growth of biominerals by various experimental methodologies,^{15,16,18,19} knowledge of the interaction between inorganic particles and the organic matrix at the molecular level is still very limited. Molecular simulation can provide useful atomistic information at this level and has already substantially contributed to our understanding of crystal nucleation and growth.^{20–23} In the present work, we have investigated the interactions between polystyrene sulfonate (PSS) and calcite surfaces by molecular dynamics (MD) simulations to provide a molecular-level explanation of the experimentally observed PSS-stabilized exposure of (001) surfaces during calcite mineralization. We investigated the adsorption behavior of short oligomers of PSS on calcite (001) and (104) surfaces and identified several factors that influence the adsorption. Free energy calculations were performed to compute adsorption strength and show the distinct binding modes of the styrene sulfonate unit on the calcite surfaces, as well as the effect of the orientation of the aromatic ring to the adsorption. In particular, we have investigated the role of solvent-induced forces and the importance of the variations of the interfacial water density variations on the different binding modes. On the basis of these results we discuss implications for the adsorption of long-chain PSS on calcite surfaces which can serve as an explanation of the experimentally observed control of surface exposure by PSS.

2. METHOD AND SIMULATION DETAILS

2.1. Calcite Surfaces and Simulated Systems. Calcite is the most stable polymorph of CaCO_3 . There are two calcite surfaces presented in the experiment of calcite growth in PSS solution in Wang et al.'s work,^{12,13} namely, the (104) and (001) surfaces. In our MD simulation, we investigated adsorption of PSS oligomers to both types of surfaces. The systems consist of a calcite slab where the respective surface is in contact with a water slab under 3D periodic boundary conditions. The thickness of the water slab in both systems is approximately 7.7 nm (for the simulated surfaces, see below, this corresponds to approximately 6000 water molecules). This thickness is large enough so that the immediate influence of the surfaces on water properties has decayed in the center of the water layer. In both systems, the surfaces were placed parallel to the xy plane and perpendicular to the z axis of the simulation boxes. The calcite slab for the (104) surface system was composed of 864 CaCO_3 formula units resulting in a thickness of approximately 2.5 nm and a surface size of approximately $4.9 \times 4.0 \text{ nm}^2$. The (001) surface system was composed of 800 CaCO_3 formula units

resulting in a thickness of approximately 2.4 nm and a surface size of approximately $5.0 \times 4.3 \text{ nm}^2$. In the case of the (104) surface, Ca^{2+} and CO_3^{2-} are located in the same layers (Figure 1, left), and this close packed, alternating arrangement of the oppositely charged ions makes the (104) surface overall nonpolar and thermodynamically the most stable one in water solution. In the case of the (001) surface, Ca^{2+} and CO_3^{2-} are situated in separate layers, leading to a strong dipole moment in the direction normal to the surface. An overall charge neutral block of CaCO_3 with the (001) surface exposed will exhibit a strong macroscopic dipole moment as illustrated in Figure 1 (middle). In the simulation this strong dipole moment in combination with the finite system size and periodic boundary conditions and PME electrostatics cause electrostatics artifacts such as an overly strong water polarization and artificially strong adsorption of PSS on this surface. To eliminate this effect, we removed half a layer of Ca^{2+} ions from the upper (001) surface of the mineral slab and added it in such a way to the lower surface of the mineral slab that the system remains charge neutral and the macroscopic dipole moment of the calcite slab in the direction normal to the surface is removed (see Figure 1, right panel). In the so constructed system one-half of each surface is rich in Ca^{2+} ions (exposing positive charges), while the other halves expose a negatively charged layer of CO_3^{2-} ions. Note that, in principle, this procedure could be extended by dividing the system further (into quarters, etc.). The effect of this will be explored at a later stage. Figure 1 shows a side view of the nonpolar (104) calcite surface, the polar (001) surface, and our (001) surface with two steps and no overall dipole moment of the mineral slab perpendicular to the surface.

2.2. Simulation Details. The package GROMACS 4.5.4 was used for all molecular dynamics simulations in this study.²⁴ Bond lengths in the CO_3^{2-} ions and in PSS are constrained by the LINCS algorithm,²⁵ while water molecules are constrained using the SETTLE algorithm.²⁶ Periodic boundary conditions are applied in all directions. For electrostatic interactions, the Particle Mesh Ewald method (PME)²⁷ was used with a grid spacing of 0.16 nm, PME order of 4, and a real space cutoff of 1.0 nm. The cutoff distance of the Lennard-Jones interactions was set to 1.0 nm. The integration time step was 2 fs, and the neighbor list was updated every 10 steps. The simulations of short oligomers (meso dimers and isotactic hexamers) of PSS on the calcite surfaces were carried out for 100 ns in an NPT ensemble. The temperature was kept constant at 300 K via a Nose-Hoover thermostat with a time coupling constant of 0.4 ps. The Parrinello-Rahman barostat was used to maintain a pressure of 1 bar, allowing only the z -dimension (normal to the surface) of the simulation box to fluctuate, with a coupling constant of 2 ps. In all simulations, Ca^{2+} and CO_3^{2-} ions were position restrained in all dimensions via a harmonic potential

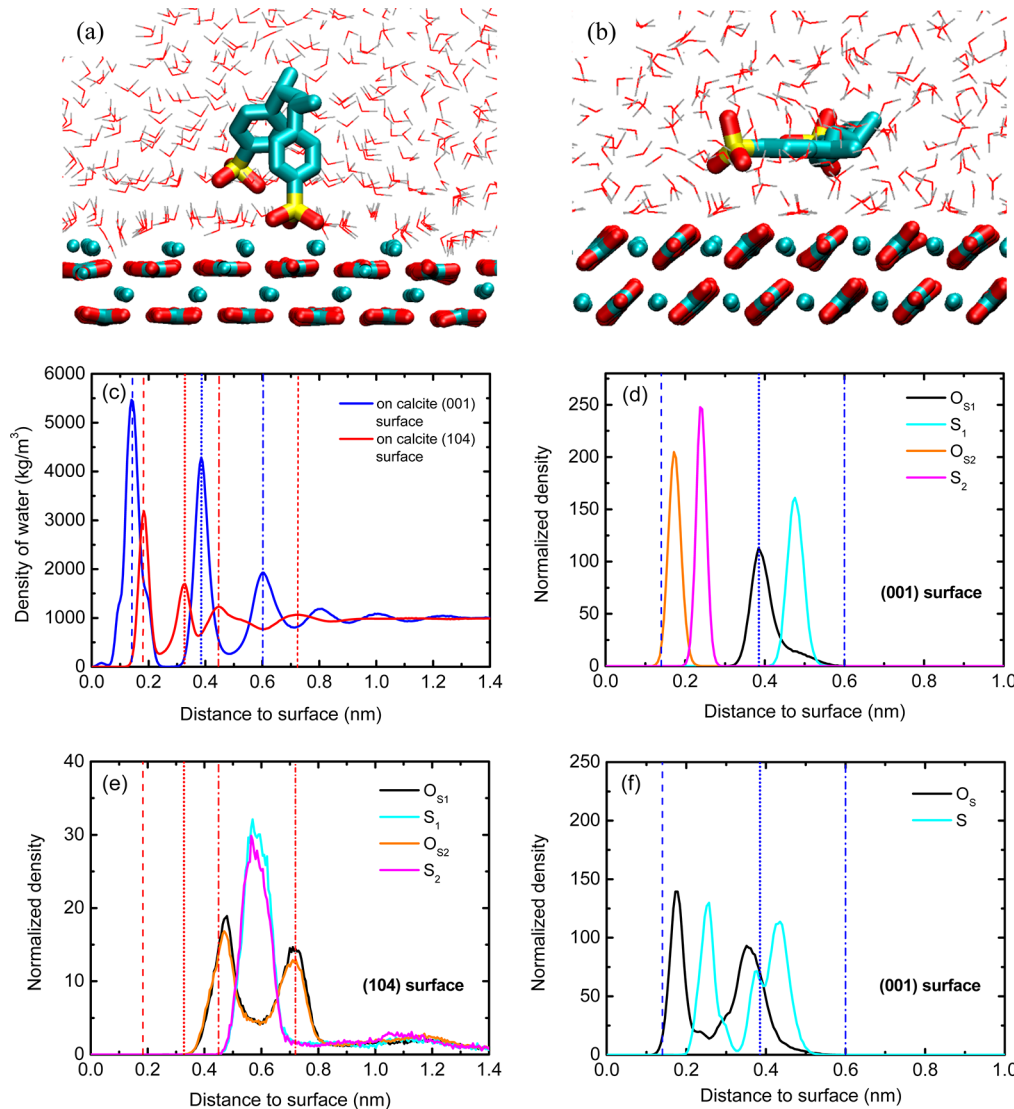


Figure 2. Snapshots of typical adsorbed states of the SS dimer on (a) the calcite (001) surface and (b) the calcite (104) surface. The SS dimer and the calcite surface are displayed by licorice mode, and water molecules are displayed as thin lines (oxygen, red; hydrogen, silver; snapshots made by VMD³⁸). (c) Water density profile normal to the calcite surfaces ((001), blue lines; (104), red lines; for the (001) surface, only the water on top of the Ca^{2+} -terminated part of the surface was accounted for). For both surfaces, the zero point, i.e., the z coordinate of the surface, was defined by the average z position of the Ca^{2+} ions in the outmost layer. The figure also shows the normalized density of the atoms of the two sulfonate groups on (d) the calcite (001) surface and (e) the calcite (104) surface and (f) the normalized density of the sulfonate groups on the calcite (001) surface averaged over 10 independent simulations (see text). All panels: perpendicular dashed and dotted lines indicate the positions of the water density maxima on the respective surface.

with a force constant of 10 000 $\text{kJ}\cdot\text{mol}\cdot\text{nm}^{-2}$ for the (001) surface and 1000 $\text{kJ}\cdot\text{mol}\cdot\text{nm}^{-2}$ for the (104) surface (for more details regarding the force field parameters see next section). For the (free) dimer simulations, the initial distance of the center of mass of the dimer to the surface was set to around 0.8 nm. Simulation trajectories were saved every 1 ps. For the calculation of the potential of mean force (PMF) of the monomer (one styrene sulfonate molecule) on both calcite surfaces, a set of umbrella sampling simulations were carried out, where the distance in z direction (perpendicular to the surface) between the center of mass of the sulfonate group and the surface (center of the top ion layer) was used as the reaction coordinate. The PMF was generated from 46 umbrella windows with a distance to the surface from 0.10 to 1.40 nm, a spacing between the windows of 0.02 nm, and a spring constant of 5000 $\text{kJ}\cdot\text{mol}^{-1}\cdot\text{nm}^{-2}$. For the calcite (001) surface, for

distances to the surface between 0.20 and 0.36 nm, the interval between umbrella windows was set to 0.01 nm, and a spring constant of 10 000 $\text{kJ}\cdot\text{mol}^{-1}\cdot\text{nm}^{-2}$ was used. In every umbrella window, 20 ns of NVT simulation was carried out (with the same thermostat settings as described above). The weighted histogram analysis method (WHAM)²⁸ was used to generate the one-dimensional free energy profile, using the last 10 ns of each trajectory for analysis.

2.3. Force Field. For the force field parameters of calcite and the calcite–water interaction, the model developed by Raiteri et al. was used.²⁹ To stay consistent with our preliminary work on the electrolyte³⁰ and polyelectrolyte (PSS) models³¹ (which are to be combined with the calcite model), we used the SPC/E water model³² (instead of the TIP4P-Ew model³³ that was used in Raiteri’s work). That implies that a slightly different partial charge on the water oxygen and hydrogen atoms was

used. The interaction strength of the nonbonded potentials for calcite–water (calcium–water and carbonate–water) interactions was maintained the same as in Raiteri's force field. In Raiteri's calcium carbonate force field, the nonbonded intra-mineral interactions and carbonate–water interactions are described by Buckingham potentials, while the nonbonded calcium–water interactions are described by a Lennard-Jones (12, 6) potential. In the present study, we fitted these Buckingham potentials to Lennard-Jones (12, 6) potentials. This conversion to Lennard-Jones interactions makes the combination with the existing (poly)electrolyte (PSS in this study) force field much more straightforward. Since these are rather severe adaptations to the original force field, we made sure that the hydration free energies of Ca^{2+} and CO_3^{2-} , the dissociation free energy profile for the $\text{Ca}^{2+}-\text{CO}_3^{2-}$ ion pair, and the water structure and density profile on the calcite (104) surface reproduce the data reported by Raiteri et al. and experiment, respectively (see Table S1 and Figures S1 and S2 in Supporting Information).²⁹ Note that the (104) mineral surface turns out to be as stable when using the LJ potentials as it is with the original Buckingham potentials. To keep the (001) surface stable, position restraints are required, a fact that is not surprising since this is a high-energy surface. Note that the converted force field with Lennard-Jones interactions might not be as suitable to reproduce the difference between different CaCO_3 polymorphs or the mineralization of different CaCO_3 phases from solution as the original combined Buckingham/Lennard-Jones sets of nonbonded parameters^{21,29}—a target of the original force field parametrization that was expendable for the present study.

The force field for PSS has been reported previously.³¹ To now combine the PSS force field with the calcite model, several cross-interaction parameters are required. Since in the mineral force field all interactions are pairwise, Lennard-Jones parameters for the atoms in the CO_3^{2-} ions are needed to apply a combination rule. Here, the OPLS-AA force field for carboxylate groups of aspartate residues was used. Likewise, the Lennard-Jones parameters of Ca^{2+} were taken from the force field of Dang and Smith.³⁴ From these atomwise Lennard-Jones parameters the cross nonbonded interactions between PSS and the mineral surface were determined by applying the geometric mixing rule.

All the parameters necessary to reproduce our atomistic simulations are summarized in the Supporting Information (Table S2). In addition, several simulations were performed to test whether the presence of counterions affects the results of this paper. For completeness, also these ion parameters and more details regarding their derivation are provided in the Supporting Information.

3. RESULTS AND DISCUSSION

In Wang and Cölfen's work of calcite growth in PSS solution, it was inferred that PSS stabilizes the unstable high-energy (001) surface, thus one would expect different binding modes and strengths of PSS to (104) and (001) surfaces. To obtain a first general impression of these binding modes, free MD simulations of meso SS dimers in contact with calcite (001) and (104) surfaces were carried out, and it was found that the adsorption behavior of the dimer is quite different for the two surfaces. Figure 2(a) and (b) shows snapshots of the typical adsorbed state of the dimer on both surfaces.

On the Ca^{2+} -terminated (001) surface, water molecules form several highly ordered, strongly polarized layers with three

major water density peaks located at 0.140, 0.385, and 0.600 nm distance from the surface, as shown in Figure 2(c). The SS dimer was rapidly adsorbed to this surface during the first several nanoseconds of simulation time. The end state of this first simulation was a configuration where one of the two sulfonate groups makes direct contact with the Ca^{2+} atoms; i.e., the sulfonate group has penetrated into the first solvation layer on the surface. This is driven by the strong electrostatic interactions between the sulfonate group and the ions in the (001) surface. This sulfonate group stays firmly adsorbed in one position during the rest of the simulation time. The other sulfonate group resides in the second solvation layer (see Figure 2(d)) and forms hydrogen bonds with the water molecules in this layer. It is relatively flexible in the x and y direction. On average this sulfonate group forms 5.5 hydrogen bonds with water, while the sulfonate group that is in contact with the surface on average only forms 1.4 hydrogen bonds with the surface water (shown in Table 1).

Table 1. Average Number of Hydrogen Bonds between the Water and Sulfonate Group in PSS^a

calcite surface	group	average no. of H-bonds
(001)	$-\text{SO}_3^{-1}$ _1	5.5
(001)	$-\text{SO}_3^{-1}$ _2	1.4
(104)	$-\text{SO}_3^{-1}$ _1	5.9
(104)	$-\text{SO}_3^{-1}$ _2	5.9
(104)	CO_3^{2-}	2.3

^aThe last row also shows the average number of hydrogen bonds between water and CO_3^{2-} in the outmost layer of the (104) surface.

On the nonpolar calcite (104) surface, water also forms several ordered high-density layers (see Figure 2(c)) with maxima at 0.183, 0.328, and 0.449 nm distance from the surface. The water is, however, not as strongly polarized as the water layer at the (001) surface. In the first layer, water molecules preferentially lie flat on the surface with the OH bonds parallel to the surface, forming hydrogen bonds with the surface CO_3^{2-} ions. The second layer of water molecules is slightly less ordered, and water forms directional (toward the surface) hydrogen bonds with the surface CO_3^{2-} ions. In total, this leads to an average of 2.3 hydrogen bonds to the surface CO_3^{2-} ions (see Table 1). These results are consistent with experimental data³⁵ and previous simulation studies.^{29,36} In the adsorbed conformation of the SS dimer, both aromatic rings lie parallel to the (104) surface. The aromatic rings as well as the sulfur atoms of both sulfonate groups are situated in a region of slightly lower water density at approximately 0.6 nm distance from the surface (see Figure 2(e)). This results in a configuration where up to four of the (in total six) oxygen atoms of the sulfonate groups can be preferentially located in the third solvation layer, interacting with the surface by forming hydrogen bonds with the ordered water molecules near the (104) surface, while the other two oxygen atoms are hydrogen bonding with the fourth solvation layer (Figure 2(e)). Both sulfonate groups form on average 5.9 hydrogen bonds with the surface water (see Table 1).

The distinct difference of the adsorption behavior of the dimer on the two surfaces probably originates from the different electrostatic interactions between the dimer and surfaces. The (001) surface is Ca^{2+} rich and thus directly binds the negatively charged sulfonate group. As shown later (Figure 3), the three sulfonate oxygen atoms can perfectly coordinate

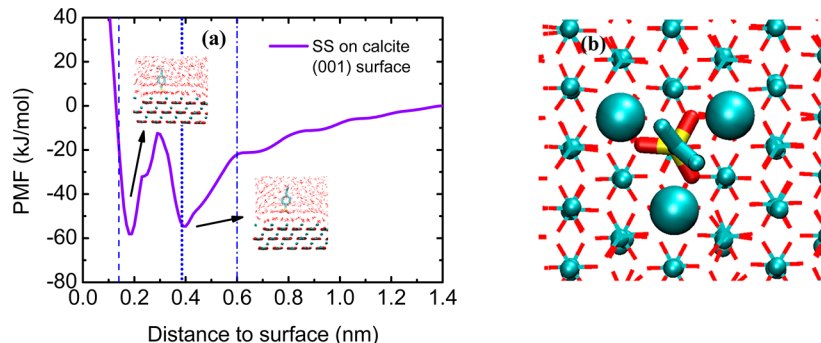


Figure 3. (a) Potential of mean force (PMF) of a monomer of PSS on the calcite (001) surface. The two deep free energy minima located at 0.18 and 0.40 nm distance correspond to the direct (contact) binding and solvent-mediated binding of the sulfonate group to the surface. The dashed and dotted lines indicate the position of the water density maxima on the (001) surface. (b) Top view of a typical adsorbed state of the monomer on the calcite (001) surface where the sulfonate group directly binds to three Ca^{2+} ions (large cyan spheres) in the top surface layer. Water molecules are omitted for clarity.

three surface Ca^{2+} ions simultaneously. In each layer of the (104) surface, on the other hand, Ca^{2+} and CO_3^{2-} ions are arranged alternately. Thus, the presence of the CO_3^{2-} ions makes the direct coordination of the sulfonate group to the Ca^{2+} ions unfavorable. An additional reason is probably the fact that the structured layers of water near this flat surface create a large barrier for surface adsorption, as was already found for other molecules.³⁷ Stable adsorption of the SS dimer to the (104) surface in a solvent-separated fashion is however favored by the possibility to form strong hydrogen bonds between the ordered water molecules and the sulfonate groups. Moreover, with the parallel orientation to the (104) surface, the aromatic ring of the SS dimer could form $\text{OH}\cdots\pi$ hydrogen bonds with water in these solvation layers. This will be discussed in more detail later.

The normalized atom densities of the two sulfonate groups on both surfaces are shown in Figure 2(d) and 2(e), and one sees that while for the (104) surface the density distributions of the two individual sulfonate groups are equivalent, on the (001) surface the two distributions are completely asymmetrical. This indicates that the system is not equilibrated since the simulation got—due to the large interaction strength—"locked" in one configuration where one sulfonate group was very stably bound to the surface and the other very stably located in the second solvation layer. This distribution does not allow an estimate of the relative strength with which the sulfonate groups bind to the two layers and whether this asymmetric binding is the only possible configuration of the dimer or whether configurations with the sulfonate groups either both in contact or both in solvent-separated binding mode are in principle also possible. To explore this a little better, 10 additional independent simulations of the SS dimer on the (001) surface were carried out. For these simulations an initial equilibration of 2 ns was carried out, where the center of mass of both sulfonate groups was constrained to a 0.3 nm distance from the surface, i.e., just in the middle between the first and second solvation layers. In the following 10 ns of simulation, the constraint was removed so that each sulfonate group could either move to the first solvation layer and bind directly to the surface Ca^{2+} ions or move to the second solvation layer. All possibly conceivable outcomes were observed in the 10 simulations: scenarios where (1) both sulfonate groups went into the contact/first solvation layer; (2) both of the sulfonate groups moved to the second solvation layer; and (3) one of the sulfonate groups moved to the contact/first solvation layer and another moved to the

second solvation layer. In all cases, the respective binding mode to the (001) surface was found to be irreversible in the simulation time. Figure 2(f) shows the resulting averaged (over these 10 simulations) normalized density of O and S atoms with respect to the (001) surface. It can be seen that the positions of the maxima of this distribution are identical to those found in the first 100 ns simulation, shown in Figure 2(d). It is clear that this average over 10 trajectories is far from being a properly equilibrated canonical probability distribution which would correspond to the free energy of binding to the surface, yet it provides a better impression of the possible (irreversible) binding modes than the first single simulation.

After this first, qualitative analysis of dimer binding from which one can deduce that the binding of a long PSS chain to the calcite (001) surface is irreversible and cannot be equilibrated, we have turned to a more quantitative analysis of the SS binding strength to the different calcite surfaces. To this end, we have calculated the potential of mean force (PMF) of a SS monomer on both surfaces. As the reaction coordinate, the distance (normal to the surface) between the center of mass of the sulfonate group and the surface was used.

Figure 3(a) shows the PMF of the monomer with respect to the calcite (001) surface. The free energy profile has two deep minima located at approximately 0.18 and 0.40 nm distance from the surface. These two minima correspond to the direct (contact) binding and solvent-mediated binding of the sulfonate group to the surface that were observed previously for the dimer. Both free energy minima are very deep, almost $-60 \text{ kJ}\cdot\text{mol}^{-1}$, i.e., substantially deeper than the thermal energy, and they are separated by a very high barrier of approximately $40 \text{ kJ}\cdot\text{mol}^{-1}$. This explains the very strong, irreversible adsorption that was observed for the dimer described above, and it also confirms the observation that thermal energy is not sufficient to allow exchanges between different binding modes. Structurally, in the first (contact) free energy minimum, the SS molecule adopts an orientation perpendicular to the surface (see inset in Figure 3(a)), and each of the three sulfonate oxygen atoms directly binds to a Ca^{2+} ion in the top surface with a perfect geometric fit, shown in the top view in Figure 3(b). In the second free energy minimum, the SS molecule is also oriented perpendicular to the surface (see inset in Figure 3(a)). Here, the position of the sulfonate group exactly coincides with the second maximum of the water density which allows optimal electrostatic interaction of the oxygen atoms with the strongly

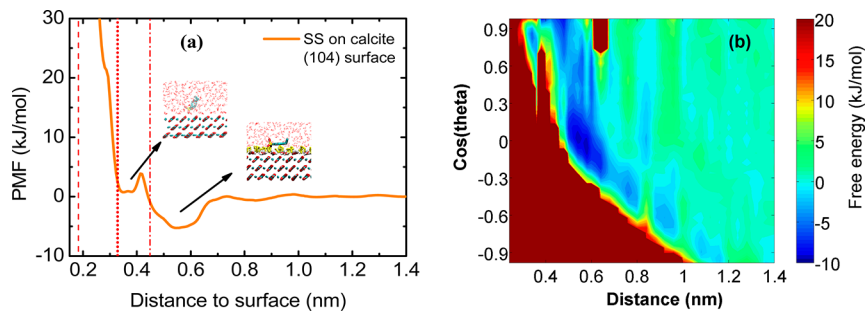


Figure 4. (a) PMF of the monomer of PSS on the calcite (104) surface. The two free energy minima located around 0.35 and 0.55 nm distance correspond to the direct (contact) binding and solvent-mediated binding of the sulfonate group to the surface. The dashed and dotted lines indicate the positions of the water density maxima on the (104) surface. (b) Two-dimensional PMF of the SS monomer on the calcite (104) surface. The two reaction coordinates are (1) distance between center of mass of sulfonate group and surface and (2) cosine of the inclination angle between the molecule and the surface normal.

polarized surface water as well as hydrogen bonding with the water molecules within this second water layer.

For the monomer on the (104) surface, there are also two free energy minima in the PMF, as shown in Figure 4(a). The free energy minimum with the sulfonate group closest to the surface corresponds to a configuration where one of the oxygen atoms of the sulfonate group directly binds to one of the Ca^{2+} ions in the top surface layer. Here, the monomer has an inclination angle with respect to the surface normal of $\approx 40^\circ$ (see also below). However, presumably due to the repulsive electrostatic interactions between the sulfonate group and the carbonate groups surrounding each Ca^{2+} ion in the top surface layer, this configuration is energetically not very favorable. The second free energy minimum is relatively broad and corresponds to the solvent-mediated binding mode of the sulfonate group that was already previously described for the SS dimer on the (104) surface, where the entire molecule, including the phenyl ring, lies flat, parallel to the surface in the region of lower water density. Note that the reaction coordinate of the PMF calculation was the distance of the sulfonate group to the surface and not the center of mass of the entire monomer. Due to the different orientations (with respect to the surface) of the molecule in the two free energy minima, the center of the molecule is further away from the surface in the free energy minimum where the sulfonate is pulled closer to the surface compared to the other free energy minimum (see insets in Figure 4a). The depth of the more stable free energy minimum is about $-5 \text{ kJ}\cdot\text{mol}^{-1}$, i.e., much smaller than the two minima in the PMF of the monomer on the (001) surface. This is consistent with the experimental observation that the presence of PSS during calcite crystal growth stabilizes the—otherwise—instable (001) surfaces, thus inhibiting growth of calcite crystals in the (001) direction and leading to exposure of these surfaces in the final crystals.^{13,39} In our simulations, both the monomer and the SS dimer adsorb to the calcite (001) surface substantially more strongly than to the (104) surface. The strong adsorption of the PSS oligomer on the (001) surface could stabilize this polar surface and thus inhibit the crystal growth in the (001) direction. Similar mechanisms have been found previously for the crystal growth of calcium oxalate modulated by preferential surface adsorption of peptides⁴⁰ and citrate.⁴¹

According to the above results, already small oligomers (even monomers) should show a strong preferential adsorption to the calcite (001) surface compared to the calcite (104) surface. It is unclear, however, if already small molecules could cause the

stabilization of the (001) surface the way it is experimentally observed for polymeric PSS or whether there is an amplification of the distinction between the two surfaces caused by polymerizing the styrene sulfonate units. To address this question, we have analyzed the simulations of the dimers and monomers on the two surfaces in more detail. To this end, we have analyzed the configurations that contribute to the various binding states of the SS monomer at the different calcite surfaces. As described above, it was found that for the adsorption to the (001) surface the monomer always remains in orientations perpendicular to the surface. This is different for the adsorption at the (104) surface. Here, the orientation of the entire unit, and most importantly of the aromatic ring, varies along the reaction coordinate in the PMF calculation, and this behavior of the aromatic ring can help to understand the critical steps of the polymer adsorption/desorption mechanism on this calcite surface. Therefore, a two-dimensional potential of mean force of the SS monomer on the calcite (104) surface was computed (see Figure 4(b))—more precisely the free energy as a function of the distance between the center of mass of the sulfonate group and the surface on the one axis and of the cosine of the inclination angle θ between the monomer (defined by the vector between the two aromatic carbon atoms that link to the backbone and the sulfonate group, respectively) and the surface normal on the other axis. When $\cos(\theta) = 1$ (or -1), the monomer is oriented perpendicular to the surface, while for $\cos(\theta) = 0$, the monomer is oriented parallel to the surface, which typically coincides with the aromatic ring being oriented parallel to the surface (see snapshot in Figure 4(a)). The 2D-PMF was obtained from constrained MD simulations with a distance constraint between the center of mass of the sulfonate group and the surface (46 runs with 20 ns simulation time each). This reaction coordinate corresponds to the one in the 1D-PMF calculations in Figure 4(a). Note that integrating the mean constraint force results again in the 1D-PMF, $G(z)$. From the conditional probability distribution of the inclination angle sampled in these constrained MD runs, one can compute the conditional free energy $G(\theta|z) = -k_{\text{B}}T \ln P(\theta|z)$, i.e., the free energy of a configuration with a certain inclination angle in the ensemble corresponding to one specific distance z to the surface. From the 1-D PMF, $G(z)$, and the conditional free energy, $G(\theta|z)$, one can now compute the 2D-PMF $G(z,\theta)$ via $G(z,\theta) = G(z) + G(\theta|z)$. The resulting free energy landscape is shown in Figure 4(b). The lowest point in this free energy landscape corresponds to $z = 0.58 \text{ nm}$ and $\cos(\theta) \approx 0$. At this position, the hydrophobic aromatic ring lies parallel to the

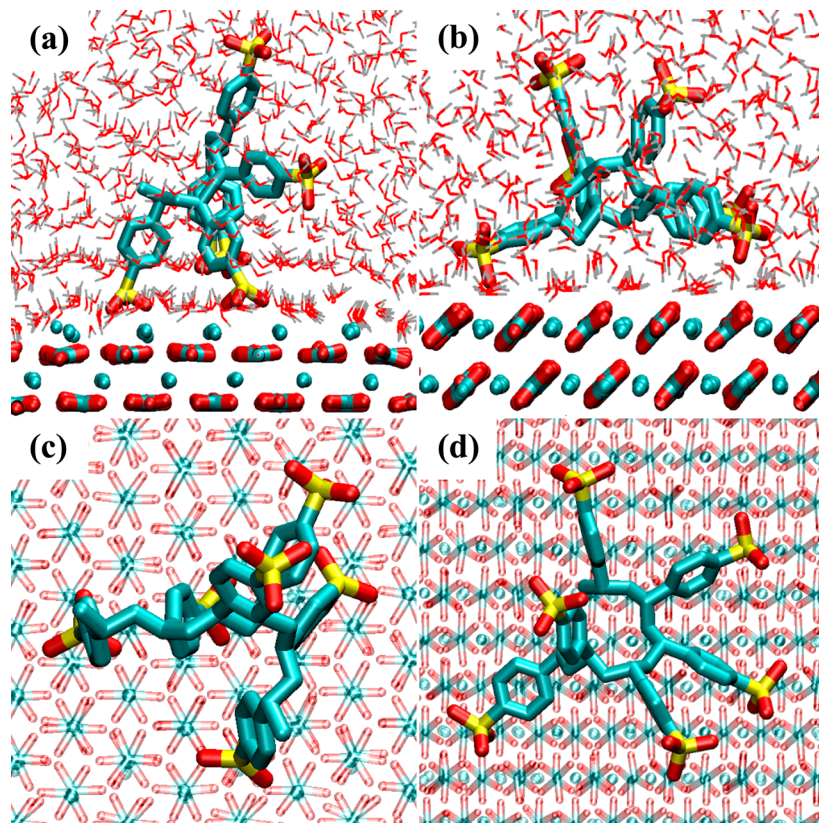


Figure 5. Side view and top view of the final (adsorbed) states of a 100 ns MD simulation of a PSS hexamer on the calcite (001) and (104) surfaces. (a) (001) surface: side view; (b) (104) surface: side view; (c) (001) surface: top view; (d) (104) surface: top view.

surface and is located in the water density minimum between the third and fourth solvation layers (see Figure 2(c)). A similar orientation of the styrene sulfonate unit had been found already in the case of the dimer (see snapshot in Figure 2(b)). In this orientation, both the sulfonate group and the aromatic ring form (in the case of the aromatic ring $\text{OH}\cdots\pi$) hydrogen bonds with the two adjacent water layers (see also Figure 2(e)). Previous simulations of uncharged aromatic amino acid residues on hydrophilic metal surfaces have indicated similar binding modes.^{42,43} Another free energy minimum is located at $z = 0.36 \text{ nm}$ and $\cos(\theta) \approx 0.76$ (i.e., an inclination angle with respect to the surface normal of $\approx 40^\circ$). At this position, one oxygen of the sulfonate group is in contact with one of the Ca^{2+} ions in the first surface layer, but the other two oxygen atoms point away from the surface due to electrostatic repulsion by the CO_3^{2-} ions (see inset of Figure 4(a)). This results in the observed inclination angle of the molecule. It should also be noted that close to the surface certain orientations of the aromatic ring are hindered, indicated by a high free energy barrier which is presumably caused by the distinct water layering. The 2D-PMF nicely shows the behavior of the aromatic ring near the calcite (104) surface, and it illustrates the significance of the orientation of the styrene sulfonate unit for the adsorption strength on this surface. This is a very important result since due to the strong orientation dependence at the (104) surface the adsorption strength of a polymer is most likely not a simple sum of the individual contributions from the monomeric units. The adsorption strength could (if at all) only be additive if all styrene sulfonate units in the polymer could be arranged optimally with respect to the surface. This is unlikely for steric reasons and because this arrangement leads to a large

distortion of the polymer conformation that is both energetically and entropically unfavorable and that would compensate a large part of the favorable adsorption free energy.

On the basis of these results, one would make the following prediction for the adsorption of a longer oligomer of PSS on the two calcite surfaces: on the (001) surface already the monomer adsorbs very strongly, and there are two very deep free energy minima in which the individual sulfonate groups can reside, one in direct contact to the surface and one in the second solvation layer. Therefore, in a polymer, several styrene sulfonate units can interact very favorably with the surface at the same time (in different orientations). Contrary to this, on the (104) surface the monomeric units are adsorbed most strongly to the surface in a configuration where the aromatic rings are aligned parallel to the surface, positioned in the low water density region between the third and fourth solvation layer. In a polymer this can be simultaneously realized only for very few units, resulting in comparatively weak adsorption. This means that the distinction between the adsorption to the two surfaces should be amplified by polymerization.

To test this hypothesis, a few preliminary tests of PSS oligomers on the two surfaces have been performed. Figure 5 shows the end states of two 100 ns MD simulations of an isotactic hexamer of PSS in the presence (initially not adsorbed) of both surfaces. The adsorption behavior of the hexamer is qualitatively similar to that of the dimer on the two surfaces. In both cases, the hexamer adsorbs to the surface, albeit much more readily in the case of the (001) surface than in the case of the (104) surface. For the (104) surface, it was also found that the adsorption was comparatively weak, so that small variations in the simulation parameters (presence of

counterions, etc.) would lead to the hexamer not adsorbing at all or being in an adsorbed/desorbed equilibrium. Figure 5(a) and (c) shows that two of the sulfonate groups of the hexamer directly bind to the calcite (001) surface with contact to the surface Ca^{2+} ions, and this can be perfectly combined with another two sulfonate groups located in the second free energy minimum (second solvation layer) interacting with the surface via hydrogen bonds. This results in a tightly bound, very rigid configuration. Figure 5(b) and (d) shows that on the (104) surface, as expected, the aromatic rings are preferentially arranged in the low-water-density region between the third and fourth solvation layer, which can be realized only by spreading the hexamer on the surface. The interaction of the (three) adsorbed sulfonate groups with the surface is mainly mediated by the solvent. The other three sulfonate groups show a larger distance to the surface, and they are very mobile, which indicates weak adsorption of the hexamer on this surface. Overall, this “spread-out”, “flat-on” binding will most likely become even more difficult for longer PSS chains. These preliminary results for the hexamer confirm our hypothesis that the adsorption strength for a PSS oligomer or polymer to the (104) surface cannot be easily extrapolated (in an additive fashion) from the monomer adsorption and that this potentially leads to an even larger difference in adsorption strength between the (104) and (001) surface for a polymer compared to a monomer. In the future we plan to extend this analysis of the adsorption of various oligomers to the two calcite surfaces and—where possible—compute binding free energies.

4. CONCLUSIONS

The adsorption behavior of styrene sulfonate monomers and PSS oligomers on calcite surfaces was studied by molecular dynamics simulations and free energy calculations. It was found that the styrene sulfonate unit binds very strongly to the calcite (001) surface in two binding modes, either via direct binding where the sulfonate oxygen can coordinate with three Ca^{2+} ions in the mineral surface or via solvent-mediated binding where the sulfonate group resides in the second layer of high water density and forms very strong hydrogen bonds with water molecules in the (strongly polarized) first and second solvation layers. In both binding modes the adsorption free energy of the monomer on the calcite (001) surface is around $60 \text{ kJ}\cdot\text{mol}^{-1}$. In contrast, the adsorption to the calcite (104) surface is much weaker, with one binding mode that is mediated by one or two layers of structured water molecules, and where the binding is strongly dependent on the orientation of the styrene sulfonate with respect to the surface. These results indicate that there is a stronger preferential binding of PSS to calcite (001) surfaces than to (104) surfaces, which explains why PSS can stabilize this—otherwise unstable—polar (001) surface and inhibits the mineral growth in the (001) direction. This agrees very well with the experimental observation that in PSS solution calcite crystals are formed where the (001) surface is exposed (which becomes more pronounced with increasing PSS concentration), while normally only the more stable (104) surface can be observed.

The simulations of monomer adsorption can already give a reasonable impression of the adsorption strength on various surfaces which can very well serve as an explanation of the stabilization of some surfaces. However, in addition, we can also show that with a closer analysis of the molecular mechanism and structural aspects of the adsorption one can explain effects that go beyond the individual monomer. We show that even in

a case where the individual monomer adsorbs favorably the adsorption energy may not be simply additive for a polymer because a favorable configuration cannot be realized for multiple monomer units when connected. This is the case for PSS oligomers on the (104) surface where the individual monomer adsorbs favorably to the surface but mostly in a configuration where the styrene sulfonate unit is oriented parallel to the surface in a low-density region of the surface water. This favorable orientation cannot be realized for multiple styrene sulfonate units simultaneously in a polymer chain; therefore, the difference in adsorption strength between the (001) and (104) surface should be amplified for the polymer compared to the individual monomer.

Summarizing, our results show how both direct (electrostatic) contact with surface ions and indirect interactions mediated by the solvent layers near the surface determine mechanism and strength of adsorption of polyelectrolytes (PSS as an example in this study) on two different calcite faces. Despite its strongly charged nature, the polar (001) surface binds PSS charged residues through solvent-induced forces which are comparably strong as direct charge-pair interactions. The importance of water density modulations for surface interactions has previously been recognized for aromatic compounds on metal surfaces^{42,43} as well as for charged amino acids interacting with metal oxides,⁴⁴ and in the present manuscript we see that even for mineral surfaces where the very strong adhesion is of electrostatic (ionic) nature the local water density plays a crucial role to define distinct binding modes and binding geometries which involve both the aromatic rings in the system as well as the charged sulfonate groups. Similar conclusions have been drawn previously from simulations of protein adhesion to nanoparticles of amorphous calcium carbonate and calcite.²²

When one approaches a complex problem such as polymer-assisted or -controlled mineralization by molecular simulations, it is important to be aware that with increasing complexity (e.g., by studying larger macromolecules instead of small fragments or by allowing rearrangements in the mineral phase) it becomes more and more difficult if not impossible to achieve a complete configurational sampling of the system and calculate free-energy related quantities. Therefore, it seems advisable to obtain well-equilibrated data for subsystems (such as oligomers on well-defined surfaces) which by themselves already give good insights into the relevant driving forces and interactions that determine the behavior of the system. With this information one can—when moving on to more complex scenarios—avoid pitfalls such as unknowingly getting stuck in ill-sampled local free energy minima. Although the nucleation and crystal growth of calcite have not been directly addressed in this work, the structural and thermodynamic information derived from the simulations provides valuable information that contributes to uncovering the physical and chemical driving forces in the adsorption/desorption of (bio)polymers on inorganic materials surfaces. This may be important to interpret experiments on biomineralization and biomimetic materials, and it may help to guide the design of (bio)polymers with specific affinity to certain surfaces which inhibits the crystal growth in certain directions, thus controlling the morphology of the crystals.

ASSOCIATED CONTENT

S Supporting Information

Validation of the adapted force field for the calcite/PSS simulation and all force field parameters in this study. This

material is available free of charge via the Internet at <http://pubs.acs.org>.

AUTHOR INFORMATION

Corresponding Author

*E-mail: peter@mpip-mainz.mpg.de.

Notes

The authors declare no competing financial interest.

ACKNOWLEDGMENTS

We would like to thank Prof. Helmut Cölfen, Christoph Globisch, Mara Jochum, and Debashish Mukherji for many helpful discussions and Davide Donadio for critical reading of the manuscript. This project has been carried out as part of the priority program SPP 1420 by the German Science Foundation. CP gratefully acknowledges support by the German Science Foundation as part of the Emmy Noether Programme.

REFERENCES

- (1) Mayer, G. Rigid Biological Systems As Models for Synthetic Composites. *Science* **2005**, *310*, 1144–1147.
- (2) Espinosa, H. G.; Juster, A. L.; Latourte, F. J.; Loh, O. Y.; Gregoire, D.; Zavattieri, P. D. Tablet-Level Origin of Toughening in Abalone Shells and Translation to Synthetic Composite Materials. *Nat. Commun.* **2011**, *2*, 173.
- (3) Ritchie, R. O. The Conflicts between Strength and Toughness. *Nat. Mater.* **2011**, *10*, 817–822.
- (4) Ji, B. H.; Gao, H. J. Mechanical Principles of Biological Nanocomposites. *Annu. Rev. Mater. Res.* **2010**, *40*, 77–100.
- (5) Espinosa, H. G.; Rim, J. E.; Barthelat, F.; Buehler, M. J. Merger of Structure and Material in Nacre and Bone – Perspectives on *De Novo* Biomimetic Materials. *Prog. Mater. Sci.* **2009**, *54*, 1059–1100.
- (6) Ruiz-Hitzky, E.; Darder, M.; Aranda, P.; Ariga, K. Advance in Biomimetic and Nanostructured Biohybrid Materials. *Adv. Mater.* **2010**, *22*, 323–336.
- (7) Kushner, A. M.; Guan, Z. B. Modular Design in Natural and Biomimetic Soft Materials. *Angew. Chem., Int. Ed.* **2010**, *50*, 9026–9057.
- (8) Sommerdijk, N. A. J. M.; de With, G. Biomimetic CaCO_3 Mineralization Using Designer Molecules and Interfaces. *Chem. Rev.* **2008**, *108*, 4499–4550.
- (9) Chen, C. L.; Qi, J. H.; Zuckermann, R. N.; DeYoreo, J. J. Engineered Biomimetic Polymers As Tunable Agents for Controlling CaCO_3 Mineralization. *J. Am. Chem. Soc.* **2011**, *133*, 5214–5217.
- (10) Pasarin, I. S.; Yang, M.; Bovet, N.; Glyvradal, M.; Nielsen, M. M.; Bohr, J.; Feidenhans'l, R.; Stipp, S. L. S. Molecular Ordering of Ethanol at the Calcite Surface. *Langmuir* **2012**, *28*, 2545–2550.
- (11) Orme, C. A.; Noy, A.; Wierzbicki, A.; McBride, M. T.; Grantham, M.; Teng, H. H.; Dove, P. M.; DeYoreo, J. J. Formation of Chiral Morphologies through Selective Binding of Amino Acids to Calcite Surface Steps. *Nature* **2001**, *411*, 775–779.
- (12) Wang, T. X.; Cölfen, H.; Antonietti, M. Nonclassical Crystallization: Mesocrystals and Morphology Change of CaCO_3 Crystals in the Presence of a Polyelectrolyte Additive. *J. Am. Chem. Soc.* **2005**, *127*, 3246–3247.
- (13) Wang, T. X.; Antonietti, M.; Cölfen, H. Calcite Mesocrystals: “Morphing” Crystal by a Polyelectrolyte. *Chem.—Eur. J.* **2006**, *12*, 5722–5730.
- (14) Song, R. Q.; Cölfen, H.; Xu, A. W.; Hartmann, J.; Antonietti, M. Polyelectrolyte-Directed Nanoparticle Aggregation: Systematic Morphogenesis of Calcium Carbonate by Nonclassical Crystallization. *ACS Nano* **2009**, *3*, 1966–1978.
- (15) Metzler, R. A.; Tribello, G. A.; Parrinello, M.; Gilbert, P. U. P. A. Asprich Peptides Are Occluded in Calcite and Permanently Disorder Biominer Crystals. *J. Am. Chem. Soc.* **2010**, *132*, 11585–11591.
- (16) Wang, X. Q.; Wu, C. M.; Tao, K.; Zhao, K.; Wang, J. Q.; Xu, H.; Xia, D. H.; Shan, H. H.; Lu, J. R. Influence of Ovalbumin on CaCO_3 Precipitation during In Vitro Biominerization. *J. Phys. Chem. B* **2010**, *114*, 5301–5308.
- (17) Marin-Garcia, L.; Frontana-Uribe, B. A.; Reyes-Grajeda, J. P.; Stojanoff, V.; Serrano-Posada, H. J.; Moreno, A. Chemical Recognition of Carbonate Anions by Proteins Involved in Biominerization Processes and Their Influence on Calcite Crystal Growth. *Cryst. Growth Des.* **2008**, *8*, 1340–1345.
- (18) Fried, R.; Mastai, Y. The Effect of Sulfated Polysaccharides on the Crystallization of Calcite Superstructures. *J. Cryst. Growth* **2012**, *338*, 147–151.
- (19) de Reese, J.; Plank, J. Adsorption of Polyelectrolytes on Calcium Carbonate – Which Thermodynamic Parameters Are Driving This Process? *J. Am. Ceram. Soc.* **2011**, *94*, 3515–3522.
- (20) Quigley, D.; Rodger, P. M. Free Energy and Structure of Calcium Carbonate Nanoparticles during Early Stages of Crystallization. *J. Chem. Phys.* **2008**, *128*, 221101.
- (21) Raiteri, P.; Gale, J. D. Water is the Key to Nonclassical Nucleation of Amorphous Calcium Carbonate. *J. Am. Chem. Soc.* **2010**, *132*, 17623–17634.
- (22) Freeman, C. L.; Harding, J. H.; Quigley, D.; Rodger, P. M. Structural Control of Crystal Nuclei by an Eggshell Protein. *Angew. Chem., Int. Ed.* **2010**, *49*, 5135–5137.
- (23) Demichelis, R.; Raiteri, P.; Gale, J. D.; Quigley, D.; Gebauer, D. Stable Prenucleation Mineral Clusters Are Liquid-Like Ionic Polymers. *Nat. Commun.* **2012**, *2*, 590.
- (24) van der Spoel, D.; Lindahl, E.; Hess, B.; Groenhof, G.; Mark, A. E.; Berendsen, H. J. C. GROMACS: Fast, Flexible, And Free. *J. Comput. Chem.* **2005**, *26*, 1701–1718.
- (25) Hess, B.; Bekker, H.; Berendsen, H. J. C.; Fraaije, J. G. E. M. LINCS: A Linear Constraint Solver for Molecular Simulations. *J. Comput. Chem.* **1997**, *18*, 1463–1472.
- (26) Miyamoto, S.; Kollman, P. A. Settle: An Analytical Version of the SHAKE and RATTLE Algorithm for Rigid Water Models. *J. Comput. Chem.* **1992**, *13*, 952–962.
- (27) Essmann, U.; Perera, L.; Berkowitz, M. L.; Darden, T.; Lee, H.; Pedersen, L. G. A Smooth Particle Mesh Ewald Method. *J. Chem. Phys.* **1995**, *103*, 8577–8593.
- (28) Kumar, S.; Rosenberg, J. M.; Bouzida, D.; Swendsen, R. H.; Kollman, P. A. The Weighted Histogram Analysis Method. *J. Comput. Chem.* **1992**, *13*, 1011–1021.
- (29) Raiteri, P.; Gale, J. D.; Quigley, D.; Rodger, P. M. Derivation of an Accurate Force-Field for Simulating the Growth of Calcium Carbonate from Aqueous Solution: A New Model for the Calcite–Water Interface. *J. Phys. Chem. C* **2010**, *114*, 5997–6010.
- (30) Shen, J. W.; Li, C.; van der Vegt, N. F. A.; Peter, C. Transferability of Coarse Grained Potentials: Implicit Solvent Models for Hydrated Ions. *J. Chem. Theory Comput.* **2011**, *7*, 1916–1927.
- (31) Li, C.; Shen, J. W.; Peter, C.; van der Vegt, N. F. A. A Chemically Accurate Implicit-Solvent Coarse-Grained Model for Polystyrenesulfonate Solutions. *Macromolecules* **2012**, *45*, 2551–2561.
- (32) Berendsen, H. J. C.; Grigera, J. R.; Straatsma, T. P. The Missing Term in Effective Pair Potentials. *J. Phys. Chem.* **1987**, *91*, 6269–6271.
- (33) Horn, H. W.; Swope, W. C.; Pitera, J. W. Development of an Improved Four-Site Water Model for Biomolecular Simulations: TIP4P-Ew. *J. Chem. Phys.* **2004**, *120*, 9665–9678.
- (34) Dang, L. X.; Smith, D. E. Comment on “Mean Force Potential for the Calcium-Chloride Ion Pair in Water” [J. Chem. Phys. 99, 4229 (1993)]. *J. Chem. Phys.* **1995**, *102*, 3483–3484.
- (35) Geissbühler, P.; Fenter, P.; DiMasi, E.; Srainer, G.; Sorensen, L. B.; Sturchio, N. C. Three-Dimensional Structure of the Calcite–Water Interface by Surface X-ray Scattering. *Surf. Sci.* **2004**, *573*, 191–203.
- (36) Kerisit, S.; Parker, S. C. Free Energy of Adsorption of Water and Metal Ions on the $\{101\bar{4}\}$ Calcite Surface. *J. Am. Chem. Soc.* **2004**, *126*, 10152–10161.
- (37) Gratz, A. J.; Hillner, P. E.; Hansma, P. K. Step Dynamics and Spiral Growth on Calcite. *Geochim. Cosmochim. Acta* **1993**, *57*, 491–495.
- (38) Humphrey, W.; Dalke, A.; Schulten, K. VMD - Visual Molecular Dynamics. *J. Mol. Graphics* **1996**, *14*, 33–38.

- (39) Geng, X.; Liu, L.; Jiang, J.; Yu, S. H. Crystallization of CaCO_3 Mesocrystals and Complex Aggregates in a Mixed Solvent Media Using Polystyrene Sulfonate As a Crystal Growth Modifier. *Cryst. Growth Des.* **2010**, *10*, 3448–3453.
- (40) Grohe, B.; O'Young, J.; Ionescu, D. A.; Lajoie, G.; Rogers, K. A.; Karttunen, M.; Goldberg, H. A.; Hunter, G. K. Control of Calcium Oxalate Crystal Growth by Face-Specific Adsorption of an Osteopontin Phosphopeptide. *J. Am. Chem. Soc.* **2007**, *129*, 14946–14951.
- (41) Grohe, B.; O'Young, J.; Langdon, A.; Karttunen, M.; Goldberg, H. A.; Hunter, G. K. Citrate Modulates Calcium Oxalate Crystal Growth by Face-Specific Interactions. *Cells Tissues Organs* **2011**, *194*, 176–181.
- (42) Schravendijk, P.; Ghiringhelli, L. M.; Delle Site, L.; van der Vegt, N. F. A. Interaction of Hydrated Amino Acids with Metal Surfaces: A Multiscale Modeling Description. *J. Phys. Chem. C* **2007**, *111*, 2631–2642.
- (43) Ghiringhelli, L. M.; Hess, B.; van der Vegt, N. F. A.; Delle Site, L. Competing Adsorption between Hydrated Peptides and Water onto Metal Surfaces: From Electronic to Conformational Properties. *J. Am. Chem. Soc.* **2008**, *130*, 13460–13464.
- (44) Schneider, J.; Ciacchi, L. C. Specific Material Recognition by Small Peptides Mediated by the Interfacial Solvent Structure. *J. Am. Chem. Soc.* **2012**, *134*, 2407–2413.